DALTON

Synthesis, properties and characterization of the trinuclear clusters $[Co_3(\mu\text{-}SR)_6(PEt_3)_3]X$ (R = Me or Et, X = BPh_4^- or PF_6^-)†

Pierluigi Barbaro,[a] Franco Cecconi,[a] Carlo A. Ghilardi,[a] Stefano Midollini,[a] Annabella Orlandini,[a] Fabrizia Fabrizi de Biani,[b] Franco Laschi[b] and Piero Zanello[b]

[a] *Istituto per lo Studio della Stereochimica ed Energetica dei Composti di Coordinazione, CNR, Via J. Nardi, 39-50132 Firenze, Italy*

[b] *Dipartimento di Chimica dell'Universita' di Siena, Pian dei Mantellini, 44-53100 Siena, Italy*

The reactions of methane- and ethane-thiol with cobalt(II) acetate in the presence of an excess of PEt_3 afforded the new clusters $[Co_3(\mu\text{-}SR)_6(PEt_3)_3]X$ (R = Me or Et, X = BPh_4^- or PF_6^-). A complete X-ray analysis of $[Co_3(\mu\text{-}SEt)_6(PEt_3)_3]BPh_4$ revealed that in the cluster cation the three cobalt atoms are at the vertices of a regular triangle, with six equivalent symmetrically bridging thiolate ligands. A multinuclear magnetic resonance study showed that the singly charged cluster molecules in solution maintain essentially the same conformation as in the solid state, the thiolate groups being involved in a rapid dynamic process. Electrochemical measurements showed that these cluster monocations undergo both a one-electron oxidation and a one-electron reduction. The latter is complicated by degradation of the corresponding neutral congeners. The electrogenerated paramagnetic compounds were studied by EPR analysis and the resulting features correlated with the results of an extended-Hückel molecular orbital study.

Transition-metal clusters are at the forefront of modern co-ordination chemistry, owing to their fascinating structural features, novel electronic properties and potential relevance to both enzymatic and industrial catalytic processes. The organothiolate anions (RS^-) and the 'naked' sulfide (S^{2-}) together with their selenium and tellurium homologues constitute fundamental building blocks in the assembly of cluster molecules.[1,2] Concerning the organothiolates in particular, the relative ease with which the S–C bonds can be cleaved as well as the possible attractive S···S interactions, which may be present in sulfur-containing complexes, greatly stimulated the interest in this kind of compound.

As a part of our investigations on transition-metal complexes with chalcogenic ligands and phosphines,[3,4] we have considered the reactions of methane- and ethane-thiol with cobalt(II) acetate in the presence of an excess of PEt_3. New diamagnetic clusters of formula $[Co_3(\mu\text{-}SR)_6(PEt_3)_3]X$ (R = Me or Et, X = BPh_4^- or PF_6^-) have been isolated and fully characterized by X-ray analysis, NMR spectroscopy, and electrochemical measurements. The electrogenerated paramagnetic species were studied through EPR and extended-Hückel molecular orbital (EHMO) analysis.

As far as we know, relatively few cobalt clusters containing mixed thiolate and phosphine ligands have so far been reported.[5,6]

Experimental

All the reactions were performed under an atmosphere of dry nitrogen. Solvents were purified and dried by standard methods. The starting materials were reagent grade used without further purification.

Syntheses

$[Co_3(\mu\text{-}SMe)_6(PEt_3)_3]BPh_4$. Triethylphosphine (1.3 cm^3, 8.8 mmol) was added to a solution of $Co(O_2CMe)_2{\cdot}4H_2O$ (1 g, 4 mmol) in dmf (dimethylformamide) (8 cm^3). Ethanol (35 cm^3) was added to the resulting solution and MeSH was bubbled through it, at room temperature, for 2 h. Addition of $NaBPh_4$ (700 mg, 2.05 mmol) dissolved in ethanol (15 cm^3) resulted in the precipitation of dark brown crystals. The complex was filtered off, washed with ethanol, then light petroleum (b.p. 40–70 °C), and dried under a current of nitrogen. Yield: 1.24 g (82% with respect to cobalt). (Found: C, 51.05; H, 7.5; Co, 15.3; S, 16.6. Calc. for $C_{48}H_{83}BCo_3P_3S_6$: C, 50.9; H, 7.4; Co, 15.6; S, 17.0%).

$[Co_3(\mu\text{-}SMe)_6(PEt_3)_3]PF_6$. A solution of $TlPF_6$ (123 mg, 0.35 mmol) in acetone (10 cm^3) was added to a solution of the above BPh_4^- salt (400 mg, 0.35 mmol) dissolved in acetone (40 cm^3). The resulting mixture was stirred at room temperature for 2 h, then the precipitate was filtered off. The filtrate was concentrated to 15 cm^3 by bubbling a stream of nitrogen at room temperature, then hexane (30 cm^3) was slowly added. Further evaporation of the solvent under a stream of nitrogen resulted in the precipitation of dark brown crystals. The complex was filtered off, washed with hexane and dried under a current of nitrogen. Yield: 250 mg (74%) (Found: C, 29.4; H, 6.5; Co, 18.0; S, 19.75. Calc. for $C_{24}H_{63}Co_3F_6P_4S_6$: C, 30.05; H, 6.6; Co, 18.45; S, 20.05%).

$[Co_3(\mu\text{-}SEt)_6(PEt_3)_3]BPh_4$. Triethylphosphine (1.3 cm^3, 8.8 mmol) was added to a solution of $Co(O_2CMe)_2{\cdot}4H_2O$ (1 g, 4 mmol) in dmf (8 cm^3). Ethanol (35 cm^3) then EtSH (0.9 cm^3, 12.2 mmol) was added. After stirring at room temperature for 2 h, the addition of a solution of $NaBPh_4$ (700 mg, 2.05 mmol) in ethanol (20 cm^3) resulted in the precipitation of dark brown crystals. The complex was filtered off, washed with ethanol, then light petroleum, and dried under a current of nitrogen. Yield: 1.3 g (80%). (Found: C, 54.15; H, 8.25; Co, 13.95; S, 15.4. Calc. for $C_{54}H_{95}BCo_3P_3S_6$: C, 53.3; H, 7.85; Co, 14.5; S, 15.8%).

$[Co_3(\mu\text{-}SEt)_6(PEt_3)_3]PF_6$. The complex was prepared with a method analogously to $[Co_3(\mu\text{-}SMe)_6(PEt_3)_3]PF_6$. Yield: 78%

† *Supplementary data available* (No. SUP 57175, 3 pp.): bonding theory and spectroscopic derivations. See Instructions for Authors, *J. Chem. Soc., Dalton Trans.*, 1996, Issue 1.

Non-SI units employed: eV ≈ 1.60 × 10^{-19} J, G = 10^{-4} T.

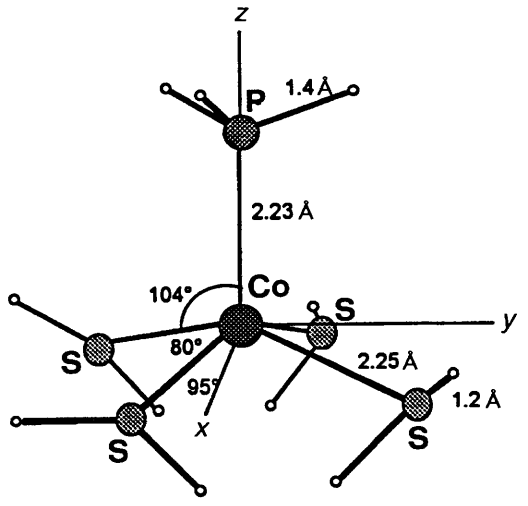

Scheme 1

(Found: C, 34.8; H, 7.45; Co, 16.75; S, 18.1. Calc. for $C_{30}H_{75}Co_3F_6P_4S_6$: C, 34.55; H, 7.25; Co, 16.95; S, 18.45%).

Crystallography

Data collection was carried out on an Enraf-Nonius CAD 4 diffractometer. Crystal data and data collection details for $[Co_3(\mu\text{-}SEt)_6(PEt_3)_3]BPh_4$ are given in Table 1. After rescaling, the intensities I were corrected for Lorentz-polarization and an empirical correction for absorption using ψ scans was applied.[7] The standard deviations $\sigma(I)$ were calculated according to ref. 8. All the calculations were carried out on a Hewlett-Packard 486 personal computer, using the SHELX 76[9] and ZORTEP[10] programs. Atomic scattering factors and anomalous dispersion factors were taken from refs. 11 (non-hydrogen), 12 (hydrogen) and 13, respectively. Patterson and Fourier maps enabled the location of all the atoms. Full-matrix least-squares refinements based on F were carried out with anisotropic thermal parameters assigned to cobalt, phosphorus and sulfur atoms. The phenyl rings were treated as rigid bodies of D_{6h} symmetry. Hydrogen atoms were introduced in their calculated positions, but not refined. During the refinement the function $\Sigma w(|F_o| - |F_o|)^2$ was minimized, w being set at $1/\sigma^2(F_o)$. Refinement converged to $R = 0.075$ and $R' = 0.076$.

Atomic coordinates, thermal parameters, and bond lengths and angles have been deposited at the Cambridge Crystallographic Data Centre (CCDC). See Instructions for Authors, *J. Chem. Soc., Dalton Trans.*, 1996, Issue 1. Any request to the CCDC for this material should quote the full literature citation and the reference number 186/245.

NMR measurements

The ^1H, ^{13}C and ^{31}P NMR spectra were recorded at 294 K on a Bruker Avance DRX-500 spectrometer operating at 500.132, 125.77 and 202.46 MHz, respectively, and equipped with a variable-temperature control unit accurate to ±0.1 °C. The ^1H and ^{13}C chemical shifts are relative to tetramethylsilane, whereas ^{31}P chemical shifts are relative to external 85% H_3PO_4 with downfield values reported as positive. The signals were assigned by two-dimensional ^1H correlation (COSY) and nuclear Overhauser effect spectroscopy (NOESY) and two-dimensional ^1H–^{13}C and ^1H–^{31}P correlations using non-spinning samples. Two-dimensional NMR spectra were recorded using pulse sequences suitable for phase-sensitive representations using time proportional phase incrementation. Double-quantum-filtered ^1H COSY experiments[14] were made with 1024 increments of size 2 K (with eight scans each) covering the full range (*ca.* 2000 Hz) in both dimensions. The ^1H NOESY measurements[15] were made with 1024 increments of size 2 K (with 16 scans each) covering the full range (*ca.* 2000 Hz) in both dimensions and a mixing time of 0.5 s. The ^1H–^{13}C correlations[16] were made using the standard heteronuclear multiple quantum coherence (HMQC) sequence with no decoupling during acquisition and 1024 increments of size 2 K (with 16 scans each) covering the 2000 Hz range in F_2 and 10 000 Hz range in F_1.

Electrochemistry and coupled EPR spectroscopy

The materials and apparatus for electrochemistry and coupled EPR spectroscopy have been described elsewhere.[17] The potentials reported refer to the saturated calomel electrode (SCE). Under the present experimental conditions the one-electron oxidation of ferrocene occurs at $E^{o\prime} = +0.44$ V. Cyclic voltammograms with scan rates varying from 0.02 to 10.24 V s^{-1} were analysed[18] to check the parameters diagnostic for electrochemical reversibility (i_{pc}/i_{pa} constantly equal to 1; $i_{pa}\,v^{-\frac{1}{2}}$ constant; ΔE_p close to 60 mV at low scan rates). The diphenylpicrylhydrazyl (dpph) free radical was used as the external magnetic field H_o marker ($g_{iso} = 2.0036$).

EHMO calculations

Extended-Hückel calculations[19,20] were performed by using either the mononuclear model complex $[Co(SH_2)_4(PH_3)]^{2+}$, Scheme 1, or the trinuclear model complex $[Co_3(SH)_6(PH_3)_3]^{n+}$ using the average of the bond lengths and angles to obtain the idealized C_{3v} symmetry. Orbital parameters were as reported in ref. 21.

Results and Discussion

The reaction of $Co(O_2CMe)_2$ with triethylphosphine (molar ratio < 1:2) with an excess of methane- (or ethane-)thiol under anaerobic conditions allowed the synthesis, in high yield, of the mixed-valence (+2.33) singly charged clusters $[Co_3(\mu\text{-}SR)_6(PEt_3)_3]^+$. Similar trimeric cobalt monocations with bridging benzene-1,2-dithiolate (bdt^{2-}) or ethane-1,2-dithiolate (edt^{2-}) have been obtained by oxygen oxidation of the corresponding neutral species, synthesized under a nitrogen atmosphere.[5,6]

In the air all the present compounds are stable in the solid state, but slowly decompose in solution.

Crystal structure

The structure of $[Co_3(\mu\text{-}SEt)_6(PEt_3)_3]BPh_4$ consists of trimeric cations $[Co_3(\mu\text{-}SEt)_6(PEt_3)_3]^+$ and tetraphenylborate anions. Fig. 1 shows a perspective view of the complex cation. Selected bond distances and angles are given in Table 2.

In this 50 valence-electron cluster cation the three cobalt atoms are at the vertices of a triangle, with six equivalent symmetrically bridging thiolate ligands. The triangle is very regular and the Co–Co bond distances, which are practically identical [range 2.575(2)–2.580(2) Å], give evidence of some metal–metal interaction. An empirical rule[22] to calculate the numbers of M–M bonds in a cluster gave a bond order of $+\frac{2}{3}$. Each cobalt atom displays a distorted square-pyramidal geometry, being surrounded by four bridging basal sulfur ligands and by a terminal triethylphosphine group in the apical site. The distortion of this from the ideal is well evidenced by the values of the basal axial angles [147.2(1)–156.6(1)°], with the three metals displaced out of the mean plane of their basal sulfur ligands towards the phosphine groups by 0.55, 0.54 and 0.52 Å, respectively.

Alternatively the six sulfur ligands can be viewed as

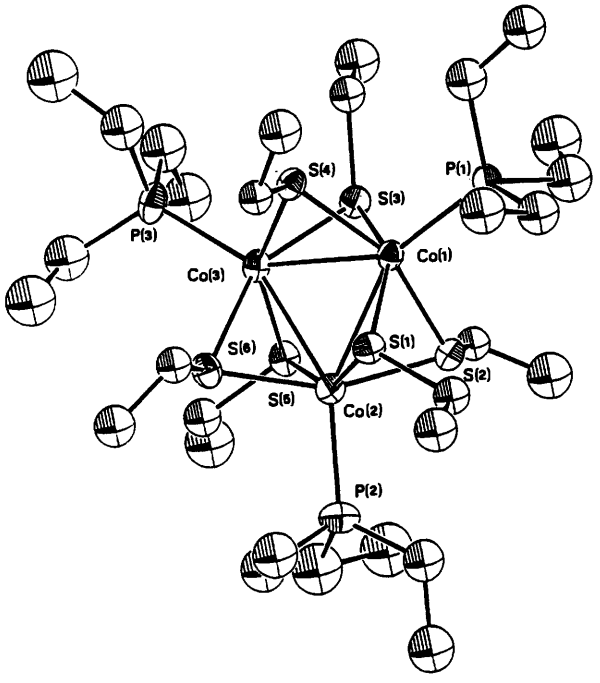

Fig. 1 Perspective view of the cluster unit $[Co_3(SEt)_6(PEt_3)_3]^+$ (ZORTEP drawing with 30% probability ellipsoids)

Table 1 Crystal data and data collection details

Formula	$C_{54}H_{95}BCo_3P_3S_6$
M	1217.27
T/K	293
Crystal symmetry	Triclinic
Space group	$P\bar{1}$
a/Å	10.477(20)
b/Å	16.821(3)
c/Å	19.101(9)
α/°	78.50(2)
β/°	74.49(6)
γ/°	77.91(5)
U/Å^3	3134.8
Z	2
D_c/g cm^{-3}	1.289
F(000)	1292
Habit	Irregular prism
Dimensions/mm	0.80 × 0.45 × 0.15
μ/cm^{-1}	10.83
Absorption correction range	0.722–1.00
Radiation	Mo-Kα, λ = 0.7107 Å
Monochromator	Graphite crystal
Scan speed/° min^{-1}	8.24–1.50
Scan width/°	0.8 + 0.35 tan θ
Background time	Half the scan time
Standards	3 every 60 min
Maximum deviation of the standards (%)	3
2θ Limits/°	5–45
Number of total data	8452
Number of data [$I > 3.5\sigma(I)$]	6432
Final number of variables	315

positioned at the vertices of a trigonal prism, with the three cobalt atoms outside the rectangular faces. Looking at the S • • • S contacts, those parallel to the pseudo-three-fold axis of the prism are short enough to suggest that some interligand sulfur–sulfur interactions could be operative [S(1) • • • S(2) 2.90, S(3) • • • S(4) 2.86 and S(5) • • • S(6) 2.86 Å; van der Waals radius of sulfur 1.85 Å]. Such a possibility has been pointed out as playing a role in the stabilization of the trigonal-prismatic geometry instead of the octahedral one.[23,24] The other S • • • S contacts, parallel to the triangular sides of the prism [range 3.02–3.59 Å], have values strictly connected with the steric arrangement of the sulfur substituents (larger S • • • S contacts

Table 2 Selected bond distances (Å) and angles (°) for $[Co_3(\mu\text{-}SEt)_6(PEt_3)_3]BPh_4$

Co(1)–Co(2)	2.580(2)	Co(3)–S(4)	2.243(3)
Co(1)–Co(3)	2.579(2)	Co(3)–S(5)	2.265(3)
Co(2)–Co(3)	2.575(2)	Co(3)–S(6)	2.245(3)
Co(1)–S(1)	2.274(3)	Co(1)–P(1)	2.229(3)
Co(1)–S(2)	2.246(3)	Co(2)–P(2)	2.228(3)
Co(1)–S(3)	2.270(3)	Co(3)–P(3)	2.243(3)
Co(1)–S(4)	2.228(3)	S(1)–C(1)	1.84(1)
Co(2)–S(1)	2.252(3)	S(2)–C(3)	1.88(1)
Co(2)–S(2)	2.253(3)	S(3)–C(5)	1.82(1)
Co(2)–S(5)	2.278(3)	S(4)–C(7)	1.86(1)
Co(2)–S(6)	2.241(3)	S(5)–C(9)	1.82(1)
Co(3)–S(3)	2.261(3)	S(6)–C(11)	1.86(1)
Co(2)–Co(1)–Co(3)	59.87(5)	P(2)–Co(2)–S(2)	100.6(1)
Co(1)–Co(2)–Co(3)	60.05(5)	P(2)–Co(2)–S(5)	105.2(1)
Co(1)–Co(3)–Co(2)	60.08(5)	P(2)–Co(2)–S(6)	102.6(1)
S(1)–Co(1)–S(2)	79.9(1)	S(3)–Co(3)–S(4)	78.8(1)
S(1)–Co(1)–S(3)	147.2(1)	S(3)–Co(3)–S(5)	83.7(1)
S(1)–Co(1)–S(4)	93.6(1)	S(3)–Co(3)–S(6)	150.6(1)
S(2)–Co(1)–S(3)	94.4(1)	S(4)–Co(3)–S(5)	150.6(1)
S(2)–Co(1)–S(4)	156.6(1)	S(4)–Co(3)–S(6)	106.2(1)
S(3)–Co(1)–S(4)	78.9(1)	S(5)–Co(3)–S(6)	78.6(1)
P(1)–Co(1)–S(1)	108.8(1)	P(3)–Co(3)–S(3)	105.3(1)
P(1)–Co(1)–S(2)	101.1(1)	P(3)–Co(3)–S(4)	98.9(1)
P(1)–Co(1)–S(3)	104.0(1)	P(3)–Co(3)–S(5)	108.5(1)
P(1)–Co(1)–S(4)	102.3(1)	P(3)–Co(3)–S(6)	102.4(1)
S(1)–Co(2)–S(2)	80.2(1)	Co(1)–S(1)–Co(2)	69.5(1)
S(1)–Co(2)–S(5)	148.2(1)	Co(1)–S(2)–Co(2)	70.0(1)
S(1)–Co(2)–S(6)	94.0(1)	Co(1)–S(3)–Co(3)	69.4(1)
S(2)–Co(2)–S(5)	94.6(1)	Co(1)–S(4)–Co(3)	70.5(1)
S(2)–Co(2)–S(6)	156.7(1)	Co(2)–S(5)–Co(3)	69.0(1)
S(5)–Co(2)–S(6)	78.4(1)	Co(2)–S(6)–Co(3)	70.1(1)
P(2)–Co(2)–S(1)	106.6(1)		

correspond to shorter C • • • C). In particular we note that the six S–C bonds point either outwards in a nearly parallel, or upwards (downwards) in a nearly perpendicular, direction to the triangle of the cobalt atoms. The arrangement of C–S bonds above the cobalt triangle is inverted for the thiolate ligands below the three metal atoms. Each pair of thiolate ligands, bridging the same metals, displays an *anti* configuration, which minimizes intramolecular non-bonding repulsions. Interestingly, in the past, stereochemical arguments had been invoked for the non-existence of the $M_3X_6Y_3$ structure containing six symmetrically bridging thiolato groups:[24] at most five such groups had been found in the complex $[Co_3(\mu\text{-}CO)(\mu\text{-}SR)_5(CO)_3]$.[24] A comparison of the latter compound with the present one shows that in the carbonyl complex the cobalt triangle is more distorted, as would be expected due to the asymmetry of the bridging ligands. The distance between the cobalt atoms bridged by one carbonyl and one thiolato group is significantly shorter [2.485(7) Å] than the others, which display the values of 2.553(7) and 2.550(6) Å.[24]

The related trinuclear complexes $[Co_3(bdt)_3(PPh_3)_3]$[25] and $[Co_3(bdt)_3(PBu_3)_3]$,[5] with bridging benzene-1,2-dithiolate ligands, show average metal–metal distances of 2.539 and 2.517 Å, respectively.

The Co–S–Co angles ranging from 69.0(1) to 70.5(1)° as well as the Co–S distances averaging 2.255(4) Å are in full agreement with literature values.

Magnetic resonance spectra

Owing to the close similarity of the methane- and ethanethiolate derivatives, the NMR studies have been performed on the relatively simpler MeS^- compound. Proton and ^{13}C NMR data for $[Co_3(SMe)_6(PEt_3)_3]PF_6$ in CD_2Cl_2 solutions are collected in Tables 3 and 4, respectively; J_{HH} and J_{HP} coupling constants have been obtained from ^1H-$\{^{31}P\}$ and ^1H homodecoupled spectra.

Table 3 Proton NMR data for $[Co_3(SMe)_6(PEt_3)_3]PF_6$[a]

Proton	Intensity	Pattern[b]	δ	J/Hz
$S(3)CH_3$, $S(5)CH_3$ (eq)	6 H	s	1.41	
$S(4)CH_3$, $S(6)CH_3$ (ax)	6 H	s	0.67	
$S(1)CH_3$ (eq)	3 H	s	1.55	
$S(2)CH_3$ (ax)	3 H	s	0.43	
$P(1)CH_2CH_3$, $P(2)CH_2CH_3$	18 H	dt	1.11	$J_{HH} = 7.6$, $J_{HP} = 15.2$
$P(3)CH_2CH_3$	9 H	dt	1.20	$J_{HH} = 7.5$, $J_{HP} = 15.1$
$P(1)CH^{\alpha}$, $P(2)CH^{\alpha}$	6 H	dqnt	2.19[c]	$J_{HH} = 7.6$, $J_{HP} = 15.1$
$P(1)CH^{\beta}$, $P(2)CH^{\beta}$	6 H	dqnt	2.04	$J_{HH} = 7.6$, $J_{HP} = 15.1$
$P(3)CH_2$	6 H	dq	2.21[c]	$J_{HH} = 7.6$, $J_{HP} = 15.2$

[a] At 500.132 MHz, 294 K, CD_2Cl_2; chemical shifts in ppm. [b] Abbreviations: s = singlet; d = doublet; t = triplet; q = quartet; qnt = quintet. [c] Partially overlapped.

Table 4 Carbon-13 NMR data for $[Co_3(SMe)_6(PEt_3)_3]PF_6$*

Carbon	δ	J/Hz
$S(3)CH_3$, $S(5)CH_3$ (eq)	8.26	$^1J_{CH} = 139.6$
$S(4)CH_3$, $S(6)CH_3$ (ax)	13.43	$^1J_{CH} = 140.2$
$S(1)CH_3$ (eq)	9.57	$^1J_{CH} = 140.1$
$S(2)CH_3$ (ax)	8.24	$^1J_{CH} = 139.2$
$P(1)CH_2CH_3$, $P(2)CH_2CH_3$	8.08	$^1J_{CH} = 125.6$, $J_{CP} = 23.3$
$P(3)CH_2CH_3$	8.55	$^1J_{CH} = 128.5$, $J_{CP} = 21.9$
$P(1)CH_2$, $P(2)CH_2$	20.78	$^1J_{CH} = 129.0$, $J_{CP} = 22.6$
$P(3)CH_2$	21.60	$^1J_{CH} = 128.8$, $J_{CP} = 22.6$

* At 125.77 MHz, 294 K, CD_2Cl_2; chemical shifts in ppm.

Table 5 Relative intensities of NOEs for $[Co_3(SMe)_6(PEt_3)_3]PF_6$[a]

Phosphine protons	SMe protons[b] δ 1.55 (3 H)	1.41 (6 H)	0.67 (6 H)	0.43 (3 H)
$P(1)CH_2CH_3$, $P(2)CH_2CH_3$	s	s	s	s
$P(3)CH_2CH_3$	—	s	s	—
$P(1)CH_2$, $P(2)CH_2$	vs	vs	vw	vw
$P(3)CH_2$	—	vs	w	—

[a] ^1H NOESY, 500.132 MHz, 294 K, CD_2Cl_2. Abbreviations: v = very, s = strong, w = weak; — no NOE. [b] Chemical shifts.

The ^1H NMR resonances observed fit well with the solid-state structure obtained from X-ray diffraction analysis for the parent compound $[Co_3(\mu\text{-}SEt)_6(PEt_3)_3]BPh_4$. On the basis of a pseudo-symmetry plane passing through the Co(3) atom and normal to the plane of the metal atoms, there are only two sets of independent phosphine ligands [P(1), P(2), P(3)] and four sets of independent SMe ligands [S(5), S(3); S(6), S(4); S(1) and S(2)]. Consistently, resonances due to two separate sets of $P(CH_2CH_3)_3$ protons [δ 1.11, P(1), P(2); 1.20, P(3); 2:1 intensity ratio] and to four SMe groups (δ 1.55, 1.41, 0.67 and 0.43; 1:2:2:1 ratio) are observed in the ^1H NMR spectrum of $[Co_3(SMe)_6(PEt_3)_3]^+$. The methylenic phosphine protons are symmetry differentiated as well between P(1), P(2) and P(3). Moreover, the hydrogens of each CH_2 group are chemically non-equivalent in the P(1), P(2) ligands. Under the present symmetry, these two hydrogens are never symmetry related in any possible conformation of the PEt_3 groups, even assuming an equal population of the rotamers. The $P(1)CH_2CH_3$ [or $P(2)CH_2CH_3$] protons are diastereotopic (giving ^1H NMR resonances at δ 2.19 and 2.04, 1:1 ratio, CH^{α} and CH^{β}). The CH_2 protons of the $P(3)Et_3$ ligand are chemically equivalent and resonate at δ 2.21 (although partially overlapped with the previous ones, they can unequivocally be located by the two-dimensional NMR experiments). All the above attributions are supported by the two-dimensional ^1H COSY and ^1H–^{13}C correlations.

All the previous observations indicate that $[Co_3(\mu\text{-}SMe)_6(PEt_3)_3]PF_6$ adopts in solution essentially the same primary structure as that found in the solid state for $[Co_3(\mu\text{-}SEt)_6(PEt_3)_3]BPh_4$. Assuming this, the thiolate methyl group resonances have been assigned on the basis of ^1H NOESY spectroscopy by observing the intensities of the NOE from the SMe protons to the PEt_3 ones. The ^1H NOESY spectrum of $[Co_3(\mu\text{-}SMe)_6(PEt_3)_3]^+$ is shown in Fig. 2, while a rough evaluation of the intensities of the ^1H NOE cross-peaks is made in Table 5. If we consider the solid-state structure of $[Co_3(\mu\text{-}SEt)_6(PEt_3)_3]BPh_4$, the thiolate ligands can be classified as equatorial [S(1), S(3), S(5)] and axial [S(2), S(4), S(6)] according to the direction of the S–C bonds with respect to the cobalt plane. The triethylphosphine groups occupy the apical co-ordination site of each metal atom and, thus, the Co–P bonds are nearly parallel to the S–C bonds of the equatorial thiolate ligands. This arrangement places the equatorial SMe protons 'closer' to the PCH_2 protons than the axial ones. Making the same assumptions for $[Co_3(\mu\text{-}SMe)_6(PEt_3)_3]^+$, we assigned the signal of the two equivalent methyls which resonate at δ 1.41 to the equatorial S(3), S(5) groups due to their very strong NOEs with the methylenic phosphine protons. On the contrary, the pair of SMe groups which resonate at δ 0.67 show only weak NOEs to the PCH_2 protons and are therefore identified as the two axial S(4), S(6) groups. Analogously, the methyls which resonate at δ 1.55 and 0.43 are assigned to the equatorial S(1)Me and to the axial S(2)Me, respectively, due to the strong NOE of the former and to the weak NOE of the latter with the diastereotopic PCH_2 protons. Some further points are worth mentioning: (*i*) the above results confirm that three equatorial and three axial thiolate ligands are present in the solution structure of $[Co_3(\mu\text{-}SMe)_6(PEt_3)_3]^+$; (*ii*) no NOEs are observed between the SMe groups. This suggests that the latter groups are arranged so as to minimize steric interaction, *i.e.* they are in an *anti* conformation as in the described crystal structure; (*iii*) the intense NOEs between the PCH_2CH_3 and SMe protons are evidence that the ethyl groups freely rotate around the P–C bonds. Finally, exchange cross-peaks between the SMe protons are found in the ^1H NOESY spectrum of $[Co_3(\mu\text{-}SMe)_6(PEt_3)_3]^+$. The exchange is selective being observed only between the axial thiolates, between the equatorial thiolates and between the two equivalent axial thiolates and the two equivalent equatorial thiolates (see Fig. 2). The only process which can account for this dynamics is a switch of the pseudo-symmetry plane from one cobalt atom to another (Scheme 2). The switch involves inversion of the conformation of the pair of bridging thiolates from axial to equatorial, but does not change the overall symmetry of the molecule. Obviously, this process also implies scrambling of the phosphine ligands which is confirmed by the exchange between the two sets of PCH_2CH_3 protons.

In conclusion, the $[Co_3(SMe)_6(PEt_3)_3]^+$ cation shares essentially the same structure found in the solid state for the related $[Co_3(SEt)_6(PEt_3)_3]^+$; nevertheless ^1H NOESY spectroscopy showed that in solution this structure is not rigid on the NMR timescale, a chemically different site being alternatively located on one cobalt atom.

The $^{31}P-\{^{1}H\}$ NMR spectra of the methane- and ethanethiolate derivatives show at room temperature a broad resonance, which at 223 K turns into two less broad signals respectively at δ 33.1 (2P) and 31.6 (1P) in the first case, at δ 27.1 (2P) and 28.2(1P) in the second. Likely, at room temperature, the dynamic process of the cluster molecule together with some coupling of P with the cobalt quadrupolar nucleus blends the two close signals into a broad band; cooling of the solution, by quenching the dynamic process and also increasing the likelihood of the ^{31}P self-decoupling, allows resolution of the two resonances.

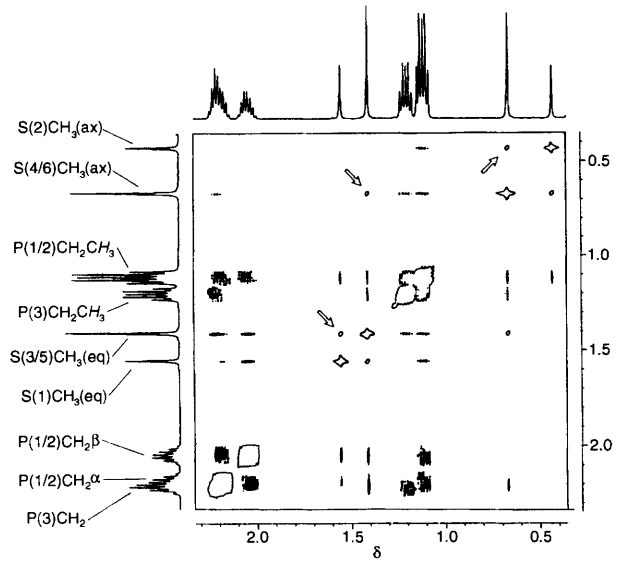

Fig. 2 The ^{1}H NOESY spectrum of $[Co_3(SMe)_6(PEt_3)_3]PF_6$ (500.132 MHz, CD_2Cl_2, 294 K); NOE cross-peaks (negative phased) are represented by filled circles, exchange cross-peaks (positive phased) by empty circles. Selective exchange peaks between thiolates are indicated by arrows

Electrochemistry

Fig. 3 shows the cyclovoltammetric patterns exhibited by complexes $[Co_3(SMe)_6(PEt_3)_3]PF_6$ **1** and $[Co(SEt)_6(PEt_3)_3]$-PF_6 **2** in dichloromethane solution. Controlled-potential coulometry shows that for both complexes the anodic step consumes one electron per molecule. In addition, cyclic voltammetry on exhaustively oxidized solutions displays voltammetric profiles quite complementary to those shown in Fig. 3. This demonstrates the chemical reversibility of the two redox changes $\mathbf{2}^{+}$–$\mathbf{2}^{2+}$ and $\mathbf{1}^{+}$–$\mathbf{1}^{2+}$, respectively. The two anodic responses show[18] substantially electrochemically reversible one-electron steps. These data are compatible with the fact that the two electrogenerated dications $\mathbf{2}^{2+}$ and $\mathbf{1}^{2+}$ essentially maintain the same geometric features as those of their monocation precursors.

The cathodic responses differ in the two cases. For $\mathbf{2}^{+}$ the reduction process does not display directly associated reoxidation peaks, except at scan rates higher than 1.0 V s^{-1}. In contrast, for $\mathbf{1}^{+}$ the i_{pc}/i_{pa} ratio = 0.8 even at 0.02 V s^{-1}. These results indicate that the decomposition of **1** is remarkably slower than that of **2**. Nevertheless, the fact that in all cases controlled-potential coulometry consumes more than three electrons per molecule and causes the profile shown in Fig. 3 to disappear confirms that the reduction process, which in the short times of cyclic voltammetry appears as a one-electron step, is complicated by subsequent chemical reactions.

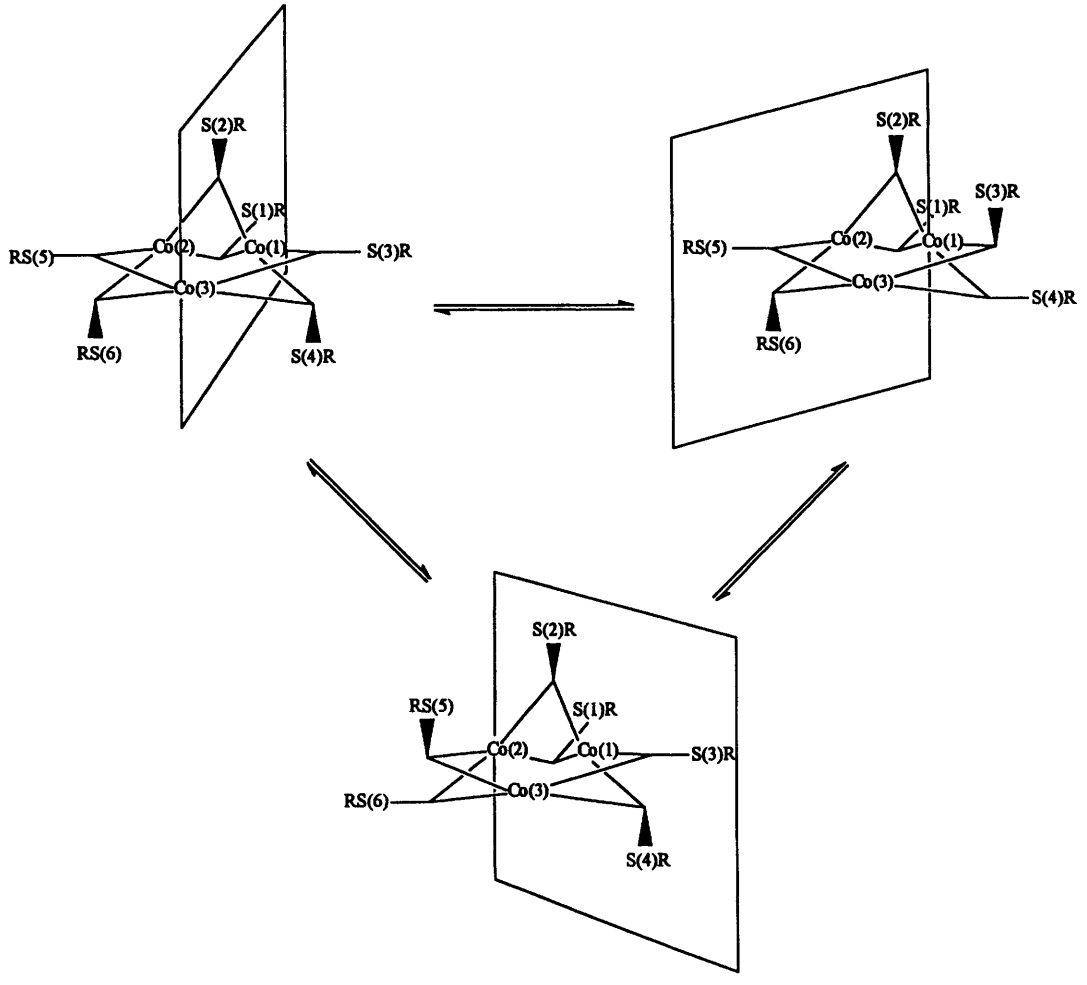

Scheme 2

Table 6 Formal electrode potentials (*vs.* SCE) and peak-to-peak separations in dichloromethane solution

Complex	$E^{\circ\prime}_{2+/+}$/V	ΔE_p[a]/mV	$E^{\circ\prime}_{+/0}$/V	ΔE_p/mV	$E^{\circ\prime}_{0/-}$/V	Ref.
$\mathbf{2}^+$ $[Co_3(SEt)_6(PEt_3)_3]^+$	+0.65	82	−1.22[b]	102[c]	—	*d*
$\mathbf{1}^+$ $[Co_3(SMe)_6(PEt_3)_3]^+$	+0.66	72	−1.24[b]	70[a]	—	*d*
$[Co_3(bdt)_3(PBu_3)_3]$			+1.04	—	−0.49	5
$[Co_3(edt)_3(PEt_3)_3]$			+0.59	—	−1.28	6[e]

[a] Measured at 0.2 V s^{-1}. [b] Followed by chemical reactions. [c] Measured at 5.12 V s^{-1}. [d] Present work. [e] In MeCN solution.

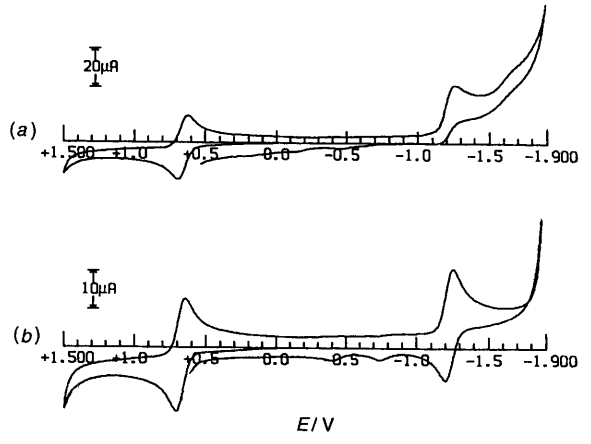

Fig. 3 Cyclic voltammetric responses recorded at a platinum electrode for CH_2Cl_2 solutions containing $[NBu_4][ClO_4]$ (0.2 mol dm^{-3}) and (*a*) $[Co_3(SEt)_6(PEt_3)_3]^+$ (9 × 10^{-4} mol dm^{-3}); (*b*) $[Co_3(SMe)_6(PEt_3)_3]^+$ (7 × 10^{-4} mol dm^{-3}). Scan rate 0.2 V s^{-1}

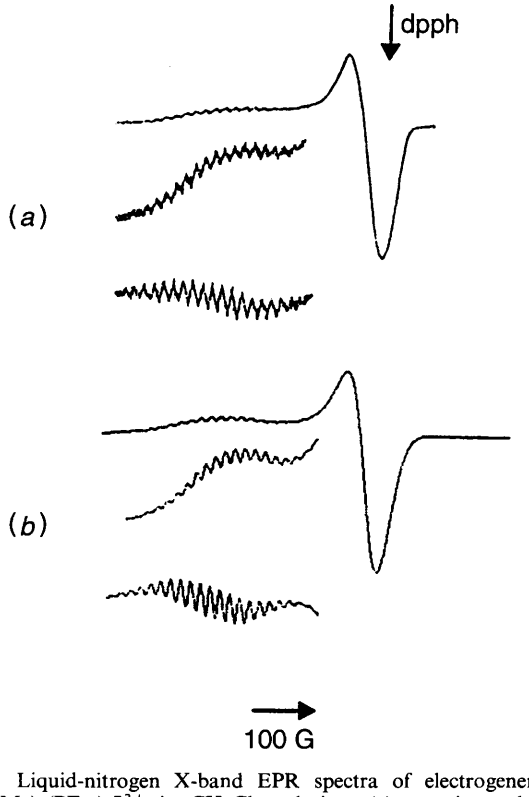

Fig. 4 Liquid-nitrogen X-band EPR spectra of electrogenerated $[Co_3(SMe)_6(PEt_3)_3]^{2+}$ in CH_2Cl_2 solution: (*a*) experimental [the enhanced signals are first (upper) and second (lower) derivative modes]; (*b*) simulated

Table 6 compiles the formal electrode potentials corresponding to the redox changes of the present thiolate complexes together with those of reported dithiolate analogues.[5,6] The manifest discrepancy is not surprising, if we consider the different nature of the sulfur ligands involved, which stabilize

Table 7 X-Band EPR parameters of the electrogenerated $[Co_3(SMe)_6(PEt_3)_3]^{2+}$ $\mathbf{1}^{2+}$, $[Co_3(SMe)_6(PEt_3)_3]$ **1** and $[Co_3(SEt)_6(PEt_3)_3]^{2+}$ $\mathbf{2}^{2+}$ species in dichloromethane solution at different temperatures;[a] *a* values are in G and refer to ^{59}Co

Complex	$g_{\parallel}$[b]	$g_{\perp}$[b]	$\langle g \rangle$[c]
$\mathbf{1}^{2+}$[d]	2.416	2.048	2.170
1	2.101	2.007	2.036
$\mathbf{2}^{2+}$	2.420	2.056	2.177

[a] $g_{\parallel,\perp}$ = 100; g_{iso} = 270 K. [b] $g_{\parallel,\perp}$ ± 0.008, $a_{\parallel,\perp}$ ± 8 G. [c] $\langle a \rangle = \frac{1}{3}(a_{\parallel} + 2a_{\perp})$, $\langle g \rangle = \frac{1}{3}(g_{\parallel} + 2g_{\perp})$. [d] g_{iso} = 2.161; $a_{\parallel}$ = 34, $a_{\perp}$ = 4 and $\langle a \rangle$ = 14 G.

compounds with different charge (the dithiolate compounds are isolated in the neutral form). Moreover, in particular, the character of the 'non-innocent' bdt ligand, which can participate in redox processes, should be taken into account.

An experimental separation of 1.9 eV between the highest occupied and lowest unoccupied molecular orbitals (HOMO-LUMO) can be computed for the two complexes studied here.

EPR analysis

Fig. 4(*a*) shows the frozen-solution X-band EPR spectrum (T = 100 K) of the electrogenerated $\mathbf{1}^{2+}$ dication. The lineshape analysis carried out in terms of an anisotropic $S = \frac{1}{2}$ spin Hamiltonian accounts for a resolved axial structure ($g_{\parallel} \gg g_{\perp} > g_e = 2.0023$). Both anisotropic regions are significantly broadened by metal-orbital contributions. Enhanced spectral resolution and second-derivative analysis of the parallel region disclosed a composite hyperfine splitting with 18 detectable lines [see inset of Fig. 4(*a*)]. Spectral simulation procedures[26] allowed us to interpret this pattern as arising from the interaction of an unpaired electron with the three equivalent cobalt nuclei ($I_{Co} = \frac{7}{2}$) of the trimetal skeleton. A structured hyperfine splitting of 22 lines is expected but line-broadening effects reduce the overall resolution to only 18. The corresponding best-fit paramagnetic parameters are collected in Table 7. There is no direct EPR evidence for the superhyperfine interaction of the unpaired electron with the apically positioned phosphorus nuclei ($I_P = \frac{1}{2}$) of the three phosphines [$a_{\parallel}(P) \ll \Delta H_{\parallel} = 27 \pm 2$ G].

At the glassy-fluid transition phase a broad and unresolved isotropic spectrum is obtained with ΔH_{iso} (270 K) = 250 ± 10 G and g_{iso} (270 K) = 2.161 ± 0.008, in good accord with the corresponding $\langle g \rangle$ = 2.170 ± 0.008. The lack of hyperfine resolution and the corresponding large ΔH_{iso} of $\mathbf{1}^{2+}$ is not surprising in the light of temperature-dependent effective relaxation mechanisms. The spectral behaviour is reversible with temperature, confirming the stability of the dication cluster under different experimental conditions.

Fig. 5(*a*) shows the frozen X-band EPR spectrum of the electrogenerated neutral complex **1** in CH_2Cl_2 solution. The lineshape analysis is consistent with the presence of a $S = \frac{1}{2}$ metal-in-character species exhibiting an axial structure ($g_{\parallel} > g_{\perp} > g_e$). The corresponding parameters are reported in Table 7. Interestingly neither cobalt or phosphorus magnetic couplings are detectable in the two anisotropic regions [$a_{\parallel}$(Co, P) $\leqslant \Delta H_{\parallel}$ = 38 ± 2 G; $a_{\perp}$(Co, P) $\leqslant \Delta H_{\perp}$ = 19 ± 2 G]. The

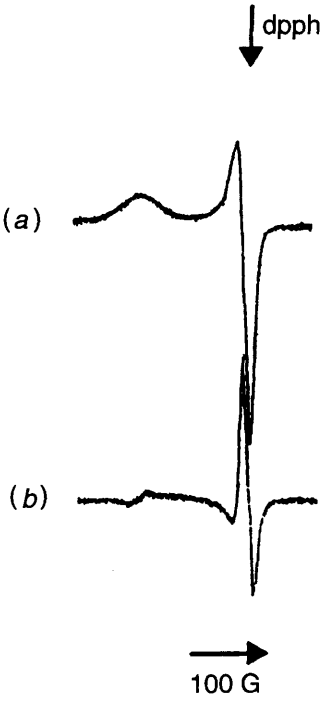

Fig. 5 Liquid-nitrogen X-band EPR spectra of electrogenerated $[Co_3(SMe)_6(PEt_3)_3]$, in CH_2Cl_2 solution: (*a*) first derivative; (*b*) second derivative

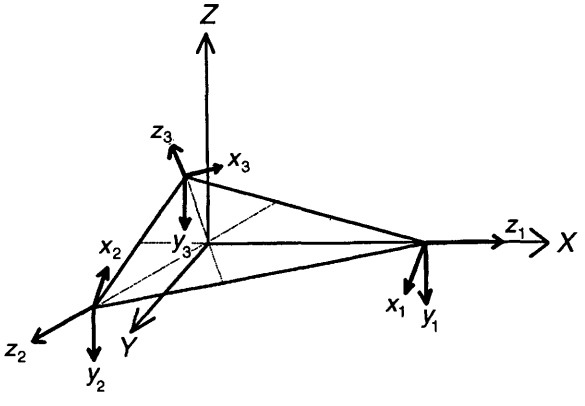

Fig. 6 Cartesian coordinate system used for the trinuclear clusters and local reference systems

lack of hyperfine resolution [Fig. 5(*b*)] reflects the different nature of the actual SOMO (singly occupied molecular orbital) with respect to that of the corresponding dication, indicating a different involvement of the cobalt atomic orbitals in it.

The glassy-fluid transition induces loss of the anisotropic signal and the solution becomes EPR silent. Only partial recovery of the axial signal was found on refreezing the neutral **1** solution, indicating lability of this compound.

The species $\mathbf{2}^{2+}$ is EPR active in glassy solution and displays a broad and axially resolved spectrum ($g_{\|} \gg g_{\perp} > g_e$) with no directly detectable cobalt couplings [$a_{\|}$(Co, P) $\leqslant \Delta H_{\|} = 35 \pm 2$ G; $a_{\perp}$(Co, P) $\leqslant \Delta H_{\perp} = 8 \pm 2$ G]; likely as a consequence of effective distortions experienced by the tricobalt cluster which cause noticeable glassy linewidths. At the glassy-fluid transition phase the paramagnetic $\mathbf{2}^{2+}$ species becomes EPR silent in the overall fluid-solution temperature range (178–300 K). The loss of a detectable isotropic spectrum is not surprising taking into account the activating effect of the temperature on the intramolecular dynamics of $\mathbf{2}^{2+}$ with the ability to induce active electron-relaxation mechanisms. Such an interpretation is confirmed by the fact that the axial lineshape is partially restored upon refreezing the $\mathbf{2}^{2+}$ fluid solution.

The different anisotropic parameters of the two dications, in particular the $g_{\|}$ components, can be interpreted by taking into account the nature of the ligand frameworks as well as the consequent molecular distortions which in turn may significantly affect the hyperfine interaction of the electron with the tricobalt skeleton.

EHMO calculations

The magnetic properties of polynuclear transition-metal clusters are usually rationalized using a Heitler–London type wavefunction, which allows the *g* and *A* tensors of the cluster to be described as a linear combination of the corresponding tensors centred on the individual paramagnetic centres,[27] even if under the 'weak bonding' approximation. Under the assumption that the present trimeric species $[Co_3(SR')_6(PR_3)_3]^{n+}$ can be described as formed by three square-pyramidal low-spin cobalt subunits, we attempted to rationalize the observed EPR features. The basic aspects of the theory and a brief discussion on the expected spectral aspects of mononuclear cobalt(II) species have been deposited (SUP. 57175).

The EPR spectra of the oxidized species $[Co_3(SR')_6(PR_3)_3]^{2+}$ are axial with hyperfine features, in the parallel region, indicative of complete delocalization of the unpaired electron. On the other hand, in these compounds, which appear as mixed-valence clusters (two Co^{III} and one Co^{II}), the three metal atoms are equivalent due to three-fold symmetry, if the bare $Co_3S_6P_3$ skeleton is considered. It ensues that the extra electron is actually expected to be delocalized over the entire ion.

Following the theoretical model proposed by Belinski and co-workers[28,29] for mixed-valence systems, we obtained expression (1) for the *g* tensor of the cluster, where g_i is the local

$$g = \tfrac{1}{3}\Sigma g_i \qquad (1)$$

g tensor expected when the extra electron is localized on the ion i. On the basis of the weak-bonding assumption, we expect g_i to be the same as in a mononuclear CoS_4P chromophore. Using equation (1) we can try to compute the local g_i tensors, assumed equivalent by symmetry arguments. Following the results of calculations on the model complex $[Co(SH_2)_4(PH_3)]^{2+}$, we assume that in the local reference system the g_i tensors are axial even if the local environment has a symmetry lower than C_{4v}. If we place the z_i principal axes parallel to the Co–P bonds and the x_i, y_i axes along the Co–S ones, see Fig. 6, we obtain relationships (2) and (3). From the experimental *g* values

$$g_{\|} = g_{i\perp} \qquad (2)$$

$$g_{\perp} = \tfrac{1}{2}g_{i\perp} + \tfrac{1}{2}g_{i\|} \qquad (3)$$

obtained for $\mathbf{1}^{2+}$ we compute $g_{i\perp} = 2.42$ and $g_{i\|} = 1.68$ for the local ion. It has previously been shown[30,31] that such values are characteristic of a ground state in which the SOMO is essentially z^2 in nature with a minor contribution from *xz* and *yz* (see SUP 57175).

As regards the hyperfine features of the dication species, the stronger observed coupling in the parallel region indicates that the *Z* axis is the unique axis common to the cluster hyperfine and *g* tensors, while there is no direct evidence for the corresponding perpendicular one. This suggests that the unpaired electron occupies a delocalized SOMO over the tricobalt plane, *i.e.* that the cobalt 3d in-plane atomic orbitals (d_{z^2} and d_{xz}) should give the highest contributions to the actual SOMO while conversely very minor contributions should arise from the cobalt 3d perpendicular-lying atomic orbitals. This interpretation reflects the overall anisotropic lineshape and particularly the resolution of the parallel region and is in accord with the previous analysis.

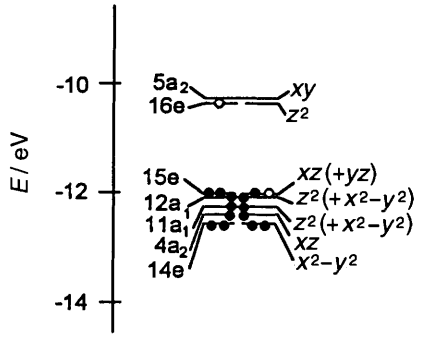

Fig. 7 Frontier orbitals computed by EH calculations on $[Co_3(SH)_6(PH_3)_3]^{n+}$ (n = 0, 1, or 2). The full circles indicate the electronic occupation for n = 2, empty circles indicate the two extra electrons subsequently added to obtain n = 1 and 0. The orbitals are labelled according to the C_{3v} symmetry of the cluster, while the metal contributions are indicated according to the local reference system. The orbitals stated in parentheses give a lower contribution

As far as the neutral congener $[CO_3(SR')_6(PR_3)_3]$ is concerned we observe a single axial $S = \frac{1}{2}$ line. As discussed in SUP 57175 the relationships (1)–(3) are valid. We compute for **1** $g_{i\perp} = 2.10$ and $g_{i\parallel} = 1.90$.

Both for $\mathbf{1}^{2+}$ and **1** the $g_{i\perp}$ *vs.* $g_{i\parallel}$ trend expected for a mononuclear square-pyramidal cobalt(II) complex is qualitatively reproduced (see SUP 57175).

Fig. 7 shows the relative energies of some high-lying orbitals of $[Co_3(SH)_6(PH_3)_3]^{n+}$ and their main composition with respect to the metal d orbitals. The orbitals are labelled according the irreducible representations of C_{3v} symmetry, while the metal contribution is labelled following the local reference system as indicated in Fig. 6. The configurations indicated follow the simple criterion of occupancy of the orbitals lower in energy and do not take account of interelectronic interactions. Accordingly, in the 2+ complex the SOMO is 15e, mainly a combination of p orbitals of the sulfur atoms with contribution from *xz* and *yz*. Taking into account interelectronic interaction, configurations other than the one shown could be lower in energy. It cannot be discounted that the SOMO could be $12a_1$ or $11a_1$, mainly z^2 in nature. These configurations give rise to the $^2A_1$ state suggested by the *g* analysis (see SUP 57175). Less doubt arises with respect to the electronic configuration of the monocation: without attempting to identify the exact nature of the HOMO, the significant HOMO–LUMO gap ($\approx$1.65 eV, in substantial agreement with the experimental value of 1.9 eV evaluated electrochemically) suggests $^1A_1$ as the fundamental state. In the neutral cluster the SOMO is 16e, z^2 in nature. This give rises to a ^2E state as suggested by the EPR analysis. The $^2A_2$ state could be similar in energy. Both 16e and $5a_2$ are antibonding orbitals, mainly with respect to the Co–Co interaction, in agreement with the experimental observation that the neutral clusters decompose at room temperature (see Experimental section). The occupation of an antibonding orbital should modify the geometry of the molecule and consequentially the energies of the MOs. The analysis of the EPR data suggests that in both the dicharged and neutral clusters the nature of the SOMO should be mainly z^2, if with a different percentage of orbital contribution. The computed g_i values of the local cobalt(II) ions are quite different. This seems to suggest that some distortion differentiates the local environment. Unfortunately since small variations in bond lengths and angles could modify the relative ordering of MOs similar in energy, in the absence of precise structural data on the 2+ and neutral clusters some uncertainty remains concerning the group-state configurations.

Acknowledgements

P. Z. gratefully acknowledges financial support by the Human Capital and Mobility Programme (EC Contract No. CHRX-CT93-0277).

References

1 I. G. Dance and K. Fisher, *Prog. Inorg. Chem.*, 1994, **41**, 637 and refs. therein.
2 I. G. Dance, *Polyhedron*, 1986, **5**, 1037.
3 C. A. Ghilardi, F. Laschi, S. Midollini, A. Orlandini, G. Scapacci and P. Zanello, *J. Chem. Soc., Dalton Trans.*, 1995, 531.
4 F. Cecconi, C. A. Ghilardi, S. Midollini, A. Orlandini, P. Zanello, A. Cinquantini, A. Bencini and M. G. Uytterhoeven, *J. Chem. Soc., Dalton Trans.*, 1995, 3881 and refs. therein.
5 B. Kang, J. Peng, M. Hong, D. Wu, X. Chen, L. Weng, X. Lei and H. Liu, *J. Chem. Soc., Dalton Trans.*, 1991, 2897 and refs. therein.
6 F. Jiang, X. Xie, B. Kang, R. Cao, D. Wu and H. Liu, *J. Chem. Soc., Dalton Trans.*, 1995, 1447 and refs. therein.
7 B. A. Frenz & Associates, Inc., College Station, Texas and Enraf-Nonius, Delft, 1985.
8 P. W. R. Corfield, R. J. Doedens, and J. A. Ibers, *Inorg. Chem.*, 1967, **6**, 197.
9 G. M. Sheldrick, SHELX 76, System of Computing Programs, University of Cambridge, 1976.
10 C. K. Johnson ORTEP, Report ORNL-5138, Oak Ridge National Laboratory, Oak Ridge, TN, 1976; as modified by L. Zsolnai and H. Pritzkow, Heidelberg University, 1994.
11 *International Tables for X-Ray Crystallography*, Kynoch Press, Birmingham, 1974, vol. 4, p. 99.
12 R. F. Stewart, E. R. Davidson and W. T. Simpson, *J. Chem. Phys.*, 1965, **2**, 3175.
13 *International Tables for X-Ray Crystallography*, Kynoch Press, Birmingham, 1974, vol. 4, p. 149.
14 A. J. Shaka and R. Freeman, *J. Magn. Reson.*, 1983, **51**, 169.
15 V. Sklener, H. Miyashiro, G. Zon, H. T. Miles and A. Bax, *FEBS Lett.*, 1986, **208**, 94.
16 M. F. Summers, L. G. Marzilli and A. Bax, *J. Am. Chem. Soc.*, 1986, **108**, 4285.
17 P. Barbaro, C. Bianchini, F. Laschi, S. Midollini, S. Moneti, G. Scapacci and P. Zanello, *Inorg. Chem.*, 1994, **33**, 1622.
18 E. R. Brown and J. Sandifer, *Physical Methods of Chemistry. Electrochemical Methods*, eds. B. W. Rossiter and J. F. Hamilton, Wiley, New York, 1986, vol. 2, ch. 4.
19 R. Hoffmann, J. R. Fujimoto, C. Swenson and C. C. Wan, *J. Am. Chem. Soc.*, 1973, **95**, 7644.
20 C. Mealli and D. M. Proserpio, *J. Chem. Educ.*, 1990, **67**, 399.
21 A. Bencini, C. A. Ghilardi, A. Orlandini, S. Midollini and C. Zanchini, *J. Am. Chem. Soc.*, 1992, **114**, 9898.
22 C. Mealli, J. A. Lopez, Y. Sun and M. J. Calhorda, *Inorg. Chim. Acta*, 1993, **213**, 199; W. P. Bosman and H. G. M. van der Linden, *J. Chem. Soc., Chem. Commun.*, 1977, 714.
23 R. Eisenberg, E. I. Stiefel, R. C. Rosenberg and H. B. Gray, *J. Am. Chem. Soc.*, 1966, **88**, 2874.
24 C. H. Wei and L. F. Dahl, *J. Am. Chem. Soc.*, 1968, **90**, 3960.
25 F. L. Jiang, X. Y. Huang, M. C. Hong, R. Cao, D. X. Wu and H. Q. Liu, *Chin. J. Chem.*, 1994, **12**, 481.
26 G. P. Lozos, B. M. Hoffman and C. G. Franz, Quantum Chemistry, Program Exchange, 1974, vol. **11**, p. 265.
27 A. Bencini and D. Gatteschi, *Electron Paramagnetic Resonance of Exchange Coupled Systems*, Springer, Berlin, 1990.
28 B. S. Tsuckerblat, M. I. Belinski and V. E. Fainzilberg, *Sov. Chem. Rev.*, 1987, **9**, 339, and refs. therein.
29 M. I. Belinski, *Mol. Phys.*, 1987, **60**, 793 and refs. therein.
30 C. Daul, C. W. Schlaepfer and A. Von Zelewsky, *Struct. Bonding (Berlin)*, 1979, **36**, 29.
31 A. Ceulemans, R. Debuyst, F. Dejehet, G. S. D. King, M. Vanhecke and L. G. Vanquickenborne, *J. Phys. Chem.*, 1990, **94**, 105; A. Ceulemans, M. Dendooven and L. G. Vanquickenborne, *Inorg. Chem.*, 1985, **24**, 1159.

Received 13*th June* 1996; *Paper* 6/04166C